

ORIGINAL RESEARCH

Molecular Dynamics and Therotyping in Airway and Gut Organoids Reveal R352Q-CFTR Conductance Defect

Sharon L. Wong^{1,2*}, Nikhil T. Awatade^{1,2*}, Miro A. Astore^{3*}, Katelin M. Allan^{1,2}, Michael J. Carnell⁴, Iveta Slapetova⁴, Po-chia Chen³, Jeffry Setiadi³, Elvis Pandzic⁴, Laura K. Fawcett^{1,2,5}, John R. Widger^{1,2,5}, Renee M. Whan⁴, Renate Griffith^{6†}, Chee Y. Ooi^{1,2,7}, Serdar Kuyucak³, Adam Jaffe^{1,2,5}, and Shafagh A. Waters^{1,2,5,8}

¹School of Women's and Children's Health, Faculty of Medicine and Health, ²Molecular and Integrative Cystic Fibrosis Research Centre, ⁴Katharina Gaus Light Microscopy Facility, Mark Wainwright Analytical Centre, ⁶School of Chemistry, and ⁸School of Medical Sciences, Faculty of Medicine and Health, University of New South Wales Sydney, Sydney, Australia; ³School of Physics, University of Sydney, Sydney, Australia; and ⁵Department of Respiratory Medicine and ⁷Department of Gastroenterology, Sydney Children's Hospital, Randwick, Australia

ORCID IDs: 0000-0001-8447-9239 (S.L.W.); 0000-0003-1560-7991 (N.T.A.); 0000-0002-9896-8831 (M.A.A.); 0000-0002-8919-5515 (K.M.A.); 0000-0003-2272-2082 (P.C.); 0000-0002-5976-2224 (J.S.); 0000-0003-3733-0890 (E.P.); 0000-0001-7069-6179 (L.K.F.); 0000-0002-9348-2760 (J.R.W.); 0000-0002-6664-6344 (R.M.W.); 0000-0001-7739-5686 (R.G.); 0000-0001-7111-0926 (C.Y.O.); 0000-0003-4315-9532 (S.K.); 0000-0002-1963-5415 (A.J.); 0000-0003-1144-5411 (S.A.W.).

Abstract

A significant challenge to making targeted cystic fibrosis transmembrane conductance regulator (CFTR) modulator therapies accessible to all individuals with cystic fibrosis (CF) are many mutations in the *CFTR* gene that can cause CF, most of which remain uncharacterized. Here, we characterized the structural and functional defects of the rare *CFTR* mutation R352Q, with a potential role contributing to intrapore chloride ion permeation, in patient-derived cell models of the airway and gut. CFTR function in differentiated nasal epithelial cultures and matched intestinal organoids was assessed using an ion transport assay and forskolin-induced swelling assay, respectively. CFTR potentiators (VX-770, GLPG1837, and VX-445) and correctors (VX-809, VX-445, with or without VX-661) were tested. Data from R352Q-CFTR were compared with data of

20 participants with mutations with known impact on CFTR function. R352Q-CFTR has residual CFTR function that was restored to functional CFTR activity by CFTR potentiators but not the corrector. Molecular dynamics simulations of R352Q-CFTR were carried out, which indicated the presence of a chloride conductance defect, with little evidence supporting a gating defect. The combination approach of *in vitro* patient-derived cell models and *in silico* molecular dynamics simulations to characterize rare *CFTR* mutations can improve the specificity and sensitivity of modulator response predictions and aid in their translational use for CF precision medicine.

Keywords: rare cystic fibrosis; personalized medicine; nasal epithelial cells; intestinal organoid; molecular dynamics simulations

Cystic fibrosis (CF), a rare, life-limiting disorder affecting ~90,000 individuals worldwide (1), results from a malfunction in the cystic fibrosis transmembrane conductance regulator (CFTR) protein. CFTR functions as a cAMP-stimulated anion

channel (2). Chloride ions diffuse through the CFTR channel pore, causing a charge imbalance that is corrected by the flux of sodium ions through sodium channels (2). The resultant ion imbalance causes osmosis of water into the extracellular space. More

than 2,000 variants in the *CFTR* gene are known. *CFTR* mutations are grouped into six major classes based on their functional defects in protein synthesis (I); intracellular maturation, processing, or folding (II); channel gating (III) or conductance

(Received in original form July 26, 2021; accepted in final form April 25, 2022)

This article is open access and distributed under the terms of the Creative Commons Attribution Non-Commercial No Derivatives License 4.0. For commercial usage and reprints, please e-mail Diane Gern.

*These authors contributed equally to this work.

†Present address: School of Natural Sciences (Chemistry), University of Tasmania, Hobart, Australia.

Supported in part by an Australian National Health and Medical Research Council grant (NHMRC_APP1188987), a Rebecca L. Cooper Foundation project grant, a Cystic Fibrosis Australia–The David Millar Giles Innovation Grant, the Sydney Children Hospital Network Foundation, and a Luminesce Alliance research grant. S.A.W. is supported by the Australian National Health and Medical Research Council. M.A.A. acknowledges support of a top-up scholarship from Cystic Fibrosis Australia. K.M.A. is supported by an Australian Government Research Training Program Scholarship. L.K.F. is supported by the Rotary Club of Sydney Cove–Sydney Children's Hospital Foundation and University of New South Wales postgraduate award scholarships.

Am J Respir Cell Mol Biol Vol 67, Iss 1, pp 99–111, July 2022

Copyright © 2022 by the American Thoracic Society

Originally Published in Press as DOI: 10.1165/rcmb.2021-0337OC on April 26, 2022

Internet address: www.atsjournals.org

activity (IV); diminished quantity (V); and diminished stability (VI) (3).

CFTR modulators can restore mutant CFTR protein function (4). Two subclasses of modulators are in current clinical use, though approval varies between countries. Potentiators such as ivacaftor (VX-770) [Kalydeco; Vertex Pharmaceuticals] increase CFTR channel gate opening. Correctors such as lumacaftor (VX-809), tezacaftor (VX-661), and elexacaftor (VX-445) increase delivery of misfolded CFTR to the cell surface. VX-809 and VX-661 are type I correctors that work by stabilizing the NBD1-TMD1 and/or NBD1-TMD2 interface by binding directly to TMD1 (5, 6). VX-445 is a type III corrector that directly stabilizes NBD1 and has been shown to have copotentiator activity (7–10). Combination therapies of potentiator and corrector(s) (Orkambi, Symdeko, Trikafta; Vertex Pharmaceuticals) are approved for use in patients with CF homozygous for F508del, the most common CFTR mutation (11–13). Trikafta is also approved for patients with CF who are heterozygous for F508del (11). The remaining patients with CF are either compound heterozygous or homozygous for mutations other than F508del, only some of which are approved for treatment with modulator therapy (14). A large number of CFTR mutations are not approved for modulator therapy, because their exact mechanism of CFTR dysfunction and/or responsiveness to modulator therapy is often unknown. Traditional randomized clinical trials of modulators to identify modulator-responsive patients with CF with rare CFTR mutations are costly, time-consuming, and impractical (15).

A major breakthrough in the field of CF has been the development of two preclinical patient- and organ-specific cell models (16–18). Both models are used in functional assays that allow rapid quantitative

measurements of CFTR function. Differentiated airway epithelial cells are used in transepithelial ion transport assays (short circuit current [I_{sc}]) (19). Intestinal organoids are used in forskolin (Fsk)-induced swelling (FIS) assays (20). Each serves as a personalized functional model of the patient's CFTR mutation and response to modulators. However, how cell models of the airway compare with those of the gut created from the same patient is not well understood. Mean changes in CFTR function *in vivo* correlate with the CFTR rescue assessed via the I_{sc} and FIS assays in cell models of subjects with the same mutations (17, 19). In addition, cell model responses in subjects with ultrarare mutations have successfully predicted clinical benefit (21–23). Results so far support the use of patient-derived cell models to guide personalized treatment (24).

We established human nasal epithelial cell (hNEC) cultures from 11 participants with wild-type functioning CFTR (WT/WT) and 10 participants with CF. The participants with CF included five participants with known and characterized CFTR folding/maturation defects (F508del/F508del), three with a CFTR synthesis defect (G542X/F508del), and one with a CFTR gating defect (G551D/F508del). The results from these CFTR mutations with a known impact on CFTR function were used as a reference and were compared with the results from one participant with the R352Q/F508del CFTR genotype. We also created matched intestinal organoids from seven participants with CF and one WT-CFTR control participant (see Table E1 in the data supplement). R352Q, a rare CFTR mutation in the CFTR channel pore, was chosen because it has been characterized in heterologous systems but is yet to be tested in a patient-derived model. Single-channel and whole-cell patch-clamp studies have demonstrated R352 to be a molecular determinant of anion selectivity and permeability in the CFTR channel pore (25). Our aims were to assess CFTR baseline

activity and CFTR modulator response in I_{sc} and FIS assays. Potentiator agents VX-770 and GLPG1837 (a potentiator in clinical trials; hereafter G1837) were tested individually and in combination with a CFTR protein-folding corrector VX-809. The effect of VX-445 as a potentiator (acute treatment) and corrector (chronic treatment) monotherapy, as well as part of triple combination therapy VX-445+VX-661+VX-770 (Trikafta) were assessed in FIS assays. In addition, to gain a complementary and better understanding of the effect of R352Q mutation on CFTR function, *in silico* structural atomistic modeling and molecular dynamics simulations were performed. Some of the results of these studies have been reported previously in the form of a preprint (<https://doi.org/10.1101/2021.08.11.456003>).

Methods

Information on materials and methods is available in the SUPPLEMENTAL MATERIALS AND METHODS section of the data supplement.

Results

R352Q-CFTR Baseline Activity and Response to CFTR Modulators in Nasal Epithelial Cells

Mature, differentiated hNECs were pseudostratified (Figure 1A) and had functional beating cilia (CBF, 6.2 ± 0.1 Hz) (Figure 1B, Video 1) and intact junction integrity (Figure 1A) (transepithelial electrical resistance, $\geq 170 \Omega \cdot \text{cm}^2$; Figure E1A). To assess ion transport, I_{sc} measurements were performed (Figures E1B–E1D). We first determined the CFTR activity threshold in reference cell models, which were used for comparison with R352Q-CFTR functional activity before and after modulator stimulation. Fsk-stimulated

Author Contributions: Conception and design: S.A.W. and A.J. Recruiting of participants: L.K.F., S.A.W., J.R.W., and C.Y.O. Collection of nasal brushings: L.K.F. and J.R.W. Human nasal epithelial cell culture and ion transport assay and analysis: N.T.A., K.M.A., and S.L.W. Immunofluorescence microscopy: S.L.W. Ciliary beat frequency (CBF) imaging: I.S. and S.L.W. CBF analysis script and design: E.P. and R.M.W. Collection of rectal biopsies: C.Y.O. Culturing the organoids: N.T.A., S.L.W., and S.A.W. Performed forskolin-induced swelling (FIS): I.S., N.T.A., K.M.A., and S.L.W. FIS assay scripts: M.J.C. FIS assay analysis: N.T.A., M.J.C., and S.L.W. Western blot analysis: S.L.W. Molecular dynamics: M.A.A., P.C., J.S., R.G., and S.K. Figure preparation: S.L.W., K.M.A., M.A.A., and S.A.W. Writing – original draft: S.L.W., M.A.A., and S.A.W. Review and editing: S.A.W., K.M.A., L.K.F., R.G., and S.K. with intellectual input from all other authors. Supervision: S.A.W. and S.K.

Correspondence and requests for reprints should be addressed to Shafagh A. Waters, Ph.D., School of Women's and Children's Health, Faculty of Medicine and Health, University of New South Wales Sydney, 418 Wallace Wurth Building, Sydney 2052, Australia. E-mail: shafagh.waters@unsw.edu.au.

This article has a data supplement, which is accessible from this issue's table of contents at www.atsjournals.org.

CFTR-dependent anion currents (ΔI_{sc-Fsk}) in WT/WT hNECs were $21.2 \pm 1.2 \mu A/cm^2$ at baseline (Figures 1C and 1D, Table E2). Baseline ΔI_{sc-Fsk} in F508del/F508del hNECs was at $3.4 \pm 0.5 \mu A/cm^2$ and was not increased beyond $\sim 0.8 \mu A/cm^2$ with either potentiator (Figure 1D). Because of the presence of two copies of the same CFTR mutation, we considered that protein expression from each of the F508del alleles was likely to be the same and therefore attributed each allele to equally contribute $\sim 1.7 \mu A/cm^2$ to baseline Fsk-stimulated currents and $\sim 0.4 \mu A/cm^2$ to potentiator-stimulated currents (Table E2). The baseline ΔI_{sc-Fsk} of G542X/F508del hNECs was $0.81 \pm 0.12 \mu A/cm^2$. Because G542X is a synthesis defect mutation with no functional CFTR protein production, the observed $\sim 0.81 \mu A/cm^2$ is attributed to the F508del allele, which is not considerably different from that calculated from the F508del/F508del hNECs. We thus used these values as a guide to estimate the contribution of the F508del allele to the experimental I_{sc} data of the heterozygous R352Q/F508del participant. In support of this, F508del/WT hNECs were previously shown to have, on average, $\sim 50\%$ of Fsk-stimulated currents of WT/WT hNECs, although variability between F508del/WT participants was present (19).

R352Q/F508del hNECs demonstrated baseline CFTR activity of $14.8 \pm 1.4 \mu A/cm^2$, an appreciable 70% of WT-CFTR activity (Figures 1C and 1D, Table E2). Potentiation with VX-770 or G1837 led to a significant ($P < 0.01$) twofold increase in CFTR activity, reaching 15.2 and 23.5 $\mu A/cm^2$ above baseline, respectively ($\sim 140\text{--}180\%$ WT-CFTR activity). This response is similar to the potentiator-stimulated response observed in the reference gating G551D/F508del hNECs. The G551D/F508del hNECs had ΔI_{sc-Fsk} of $4.9 \pm 0.6 \mu A/cm^2$ at baseline, and treatment with either potentiator caused an approximately twofold increase in CFTR activity above baseline (net increase, VX-770, 3.0 $\mu A/cm^2$; G1837, 8.1 $\mu A/cm^2$) (Figures 1C and 1D, Table E2). The majority of the response to potentiators in R352Q/F508del hNECs was most likely contributed by the restored R352Q, because the total response is far greater than the $0.4 \mu A/cm^2$ that we estimated to be attributed to the F508del allele (Figure 1D). We conclude that R352Q-CFTR has high baseline activity amenable to potentiator rescue in hNECs.

We next explored whether corrector monotherapy or cotherapy with potentiators increased R352Q-CFTR functional rescue. In F508del/F508del-CFTR cultures pretreated with VX-809, Fsk alone significantly ($P < 0.0001$) enhanced CFTR-mediated Cl^- currents by 3.7-fold, reaching $9.0 \mu A/cm^2$ above baseline (Figures 1C and 1D, Table E2). We estimated each of the F508del alleles to equally contribute $4.5 \mu A/cm^2$ to this increase in current. VX-809 cotherapy with either VX-770 or G1837 significantly ($P < 0.0001$) increased the currents stimulated by potentiator monotherapy by $\sim 10 \mu A/cm^2$ (Figure 1D). In G542X/F508del hNECs, treatment with VX-809 resulted in a modest but significant ($P < 0.0001$) increase in Fsk-stimulated currents by $1.04 \mu A/cm^2$ above baseline (Figures 1C and 1D, Table E2). In G551D/F508del hNECs, VX-809 treatment significantly ($P < 0.001$) increased CFTR activity by $5.4 \mu A/cm^2$ above baseline (Figures 1C and 1D, Table E2). Because G551D mutation does not respond to VX-809 treatment (26), the contribution of the F508del allele was considered to be $5.4 \mu A/cm^2$, similar to that calculated from the F508del/F508del hNECs. In addition, VX-809 cotherapy with either VX-770 or G1837 also increased the respective potentiator monotherapy currents by $2.7 \mu A/cm^2$ and $3.8 \mu A/cm^2$, respectively (Figure 1D). Unlike F508del/F508del-CFTR, the $9.1 \mu A/cm^2$ increase in R352Q/F508del CFTR activity from the baseline in response to VX-809 monotherapy was not statistically significant ($P = 0.09$). VX-809 cotherapy with either potentiator also resulted in a nonsignificant increase in VX-770- or G1837-potentiated CFTR currents by $\sim 2 \mu A/cm^2$ (Figure 1D). Because VX-809 does not rescue R352Q, then R352Q-CFTR is unlikely to have a folding/maturation defect. The modest increase in current with VX-809 treatment was mostly if not fully imparted by the rescued F508del allele in the R352Q/F508del hNECs.

R352Q-CFTR Baseline Activity and Response to CFTR Modulators in Intestinal Organoids

We evaluated CFTR activity in matched intestinal organoids from the same participant with the R352Q/F508del genotype and those participants with reference F508del/F508del, G551D/F508del, and WT/WT genotypes using an FIS assay. To detect baseline and modulator-stimulated CFTR activity in the organoids, swelling was

assessed at four Fsk concentrations ranging from 0.02 to 5 μM . FIS of organoids was dependent on Fsk dose, CFTR genotype, and the individual participant (Figure 2A). At 0.8 μM Fsk, the optimal concentration for baseline FIS assessment (17), minimal swelling was observed for the F508del/F508del (area under the curve [AUC], 42.8 ± 19.4) and G551D/F508del organoids (AUC, 82.9 ± 20.1) (Figure 2A). R352Q/F508del and WT/WT organoids showed considerably higher FIS at the same 0.8 μM Fsk concentration, with AUCs of 196.3 ± 19.9 and 578.3 ± 61.6 , respectively (Figure 2A).

FIS of intestinal organoids at 0.128 μM Fsk has been demonstrated to correlate strongly with clinical modulator responses and therefore is used to assess CFTR modulator response *in vitro* (17). At this Fsk concentration, organoids—*independent of CFTR genotype*—did not demonstrate FIS greater than AUC of 67.1 (Figures 2B and 2C, Table E3, Figure E2). In F508del/F508del organoids, treatment with either VX-770 or G1837 did not induce any swelling, suggesting no improvement in CFTR activity with potentiator therapy. G551D/F508del organoids showed a modest 1.5-fold increase in FIS after treatment with either potentiator, increasing AUC by 38.9 (VX-770) and 54.2 (G1837) above baseline (Figure 2C, Table E3). In WT/WT organoids, potentiation with both VX-770 and G1837 led to a significant ($P < 0.001$) increase in FIS, increasing AUC by 580.6 and 594.2 above baseline, respectively (Figure 2C). In R352Q/F508del organoids, potentiation with either VX-770 or G1837 led to a significant increase in FIS, increasing AUC by 234.6 and 910.6 above baseline, respectively (Figures 2B and 2C). G1837 was significantly ($P < 0.0001$) more effective in increasing FIS when compared with VX-770 in R352Q/F508del organoids, but not in organoids with the other CFTR genotypes, wherein the efficacy of the potentiators did not significantly differ from each other (Figure 2C, Table E3). Consistent with previous studies showing that VX-445 potentiates CFTR activity but is less potent than VX-770 (7–9), acute treatment of VX-445 modestly increased FIS in R352Q/F508del organoids by an AUC of 90.6 above baseline, lower than the AUC of 234.6 above baseline observed with VX-770 treatment (Figures 2B and 2C). As expected, acute treatment of

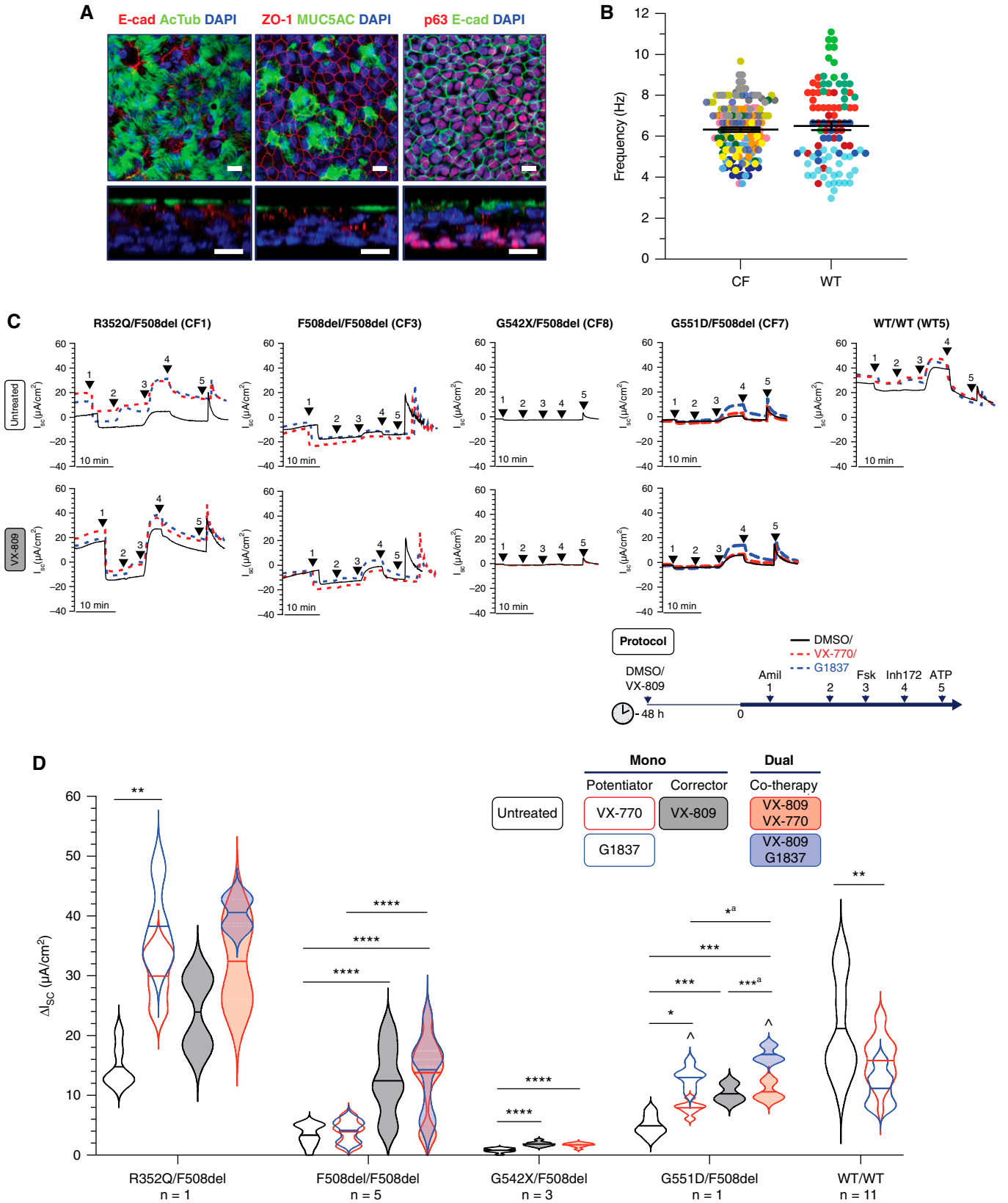


Figure 1. Functional response of R352Q-CFTR to cystic fibrosis transmembrane conductance regulator (CFTR) modulators in differentiated human nasal epithelial cells (hNECs). (A) Immunofluorescence staining of acetylated tubulin (ciliated cells), MUC5AC (goblet cells), and p63

VX-445 did not induce swelling in F508del/F508del organoids. These data indicate that R352Q has residual CFTR function and is responsive to VX-770 and G1837.

We next determined the effect of VX-809 monotherapy and cotherapy in R352Q/F508del organoids. In reference F508del/F508del and G551D/F508del organoids, VX-809 monotherapy at 0.128 μ M Fsk concentration did not yield a significant change in FIS, with a net increase in AUC \leq 30.4 above baseline (Figure 2C, Table E3, Figure E2). In F508del/F508del organoids, VX-809 cotherapy with either VX-770 or G1837 caused a significant ($P < 0.01$) increase in FIS compared with potentiator monotherapy, with a net increase in AUC of 189.3 and 145.6, respectively (Figure 2C, Table E3). In contrast, no additional increase in FIS was observed in G551D/F508del organoids after cotherapy with VX-809 and either potentiator (Figure 2C). Similar to the reference F508del/F508del organoids, no change in FIS was observed in the R352Q/F508del organoids at 0.128 μ M Fsk with VX-809 monotherapy. The net increase in AUC was 17.7 above baseline (Figures 2B and 2C, Table E3). VX-809 cotherapy in R352Q/F508del organoids followed the same trend as the F508del/F508del organoids but with a larger magnitude of response. VX-809 cotherapy with VX-770 or G1837 increased FIS beyond each respective monotherapy by 355.2 and 459.7 (Figures 2B and 2C).

The effect of VX-445 monotherapy as a corrector and VX-445+VX-661+VX-770 (Trikafta) triple combination therapy were tested in R352Q/F508del and F508del/F508del organoids. Similar to VX-809 monotherapy, VX-445 monotherapy at

0.128 μ M Fsk induced minimal FIS in R352Q/F508del and F508del/F508del organoids, increasing AUC by 101.3 and 15.2 above baseline, respectively (Figures 2A–2C). In contrast, triple combination therapy VX-445+VX-661+VX-770 significantly induced FIS in R352Q/F508del and F508del/F508del organoids, increasing AUC by 2,913 and 3,173 above baseline, respectively. Because VX-445+VX-661+VX-770 primarily targets F508del folding and processing defects, the lower magnitude of CFTR correction in R352Q/F508del organoids than in F508del/F508del organoids supports our hypothesis that R352Q is unlikely to have folding and processing defects and that the functional correction observed is likely attributed to the F508del mutation.

Correlation of CFTR Modulator Response in hNECs with Participant-matched Intestinal Organoid Swelling Assay Outcomes

We compared the CFTR modulator response as determined by ion transport in hNECs and FIS in intestinal organoids. To determine the amount of modulator-stimulated restoration above the baseline CFTR activity, we subtracted the $\Delta I_{sc}/AUC$ values with Fsk alone from those with Fsk plus modulators. A linear positive correlation was observed ($r = 0.75$; $P < 0.0001$) (Figure 3A). Participant-to-participant variability was evident (Figure 3B, Figure E3). Among the modulators, an inverse correlation was observed in response to VX-809 monotherapy between the two cell models ($r = -0.74$) (Figure 3C). Although VX-809 monotherapy significantly increased baseline currents in hNECs, no increase in FIS was detected in the matched organoids (Figure E3). When comparing

CFTR_{inh-172}-inhibited currents in hNECs against FIS in intestinal organoids, a similar trend of linear correlation was observed ($r = -0.52$; $P < 0.01$) (Figures 3A–3C).

Maturation of R352Q-CFTR in Nasal Epithelial Cells and Intestinal Organoids

We next compared CFTR maturation in R352Q/F508del hNECs and intestinal organoids, with and without VX-809 treatment, to understand the distinct response of the two cell models to VX-809 monotherapy (Figure 3D). Robust expression of mature, complex-glycosylated CFTR at \sim 160 kD (band C) was detected in both untreated and VX-809-treated hNECs and intestinal organoids. Immature, core-glycosylated CFTR at \sim 130 kD (band B) was not present. This validates our functional data by showing the presence of mature CFTR channels on the cell surface in R352Q/F508del hNECs and intestinal organoids, which can therefore elicit residual CFTR function and also respond to potentiator (acts on protein at the cell surface). Mature CFTR in intestinal organoids migrated slightly farther (lower molecular weight) than the hNECs, likely because of different processes of CFTR glycosylation in different tissues, which has been reported previously (27). Treatment with VX-809 did not further increase the levels of mature CFTR relative to the untreated control in both hNECs (densitometry/ $\times 10^4$ of 2.2 vs. 2.0) and intestinal organoids (densitometry/ $\times 10^4$ of 2.9 vs. 3.1). This is consistent with the nonsignificant or lack of functional rescue with VX-809 monotherapy in R352Q/F508del hNECs and intestinal organoids, respectively. It is noted that the intestinal

Figure 1. (Continued). (basal progenitor cells) in hNECs derived from a R352Q/F508del participant (CF1). E-cadherin (adherens junction) and ZO-1 (tight junction) are localized to the intercellular junctions of epithelial cells. The top panels are top views and the bottom panels are side views showing the pseudostratified epithelium. A 63 \times /1.4 numerical aperture oil immersion objective was used. Scale bars, 10 μ m. (B) Dot plots of mean ciliary beat frequency (CBF) measurements (Hz) of the fully differentiated mature hNECs from participants with cystic fibrosis (CF) and without CF (wild type [WT]). Each participant is coded with a different color. Each dot represents a single field of view of CBF measurement. (C) Representative Ussing chamber recordings of short circuit current (I_{sc}) in hNECs from participants with CF and WT-CFTR control participants. The protocol used to measure functional CFTR expression in hNECs in 0.01% DMSO vehicle (untreated; top) or pretreated with corrector (3 μ M VX-809 for 48 h; bottom) followed by sequential addition of 100 μ M apical amiloride (1. Amil), apical addition of either vehicle control 0.01% DMSO (black) or 10 μ M VX-770 (red) or 10 μ M G1837 (blue) (2. DMSO, VX-770, G1837), 10 μ M basal forskolin (3. Fsk), 30 μ M apical CFTR inhibitor (4. CFTR_{inh-172}), and 100 μ M apical ATP (5. ATP). A basolateral-to-apical chloride gradient was used. (D) Violin plots of total currents stimulated by DMSO or VX-770 or G1837 plus Fsk in hNECs untreated or pretreated with VX-809. Data are from 1 R352Q/F508del participant, 5 F508del/F508del participants, 3 G542X/F508del participants, and 1 G551D/F508del participant with CF and 11 WT-CFTR control participants. n, number of participants. Data are represented as violin plots to show the distribution of data. One-way ANOVA was used to determine statistically significant differences. * $P < 0.05$, ** $P < 0.01$, *** $P < 0.001$, and **** $P < 0.0001$. ^a P for G1837 only. ^b P for G1837 vs VX-770. Where VX-770 and G1837 (overlapping violin plots) both achieved statistical significance, the least significant P value is shown.

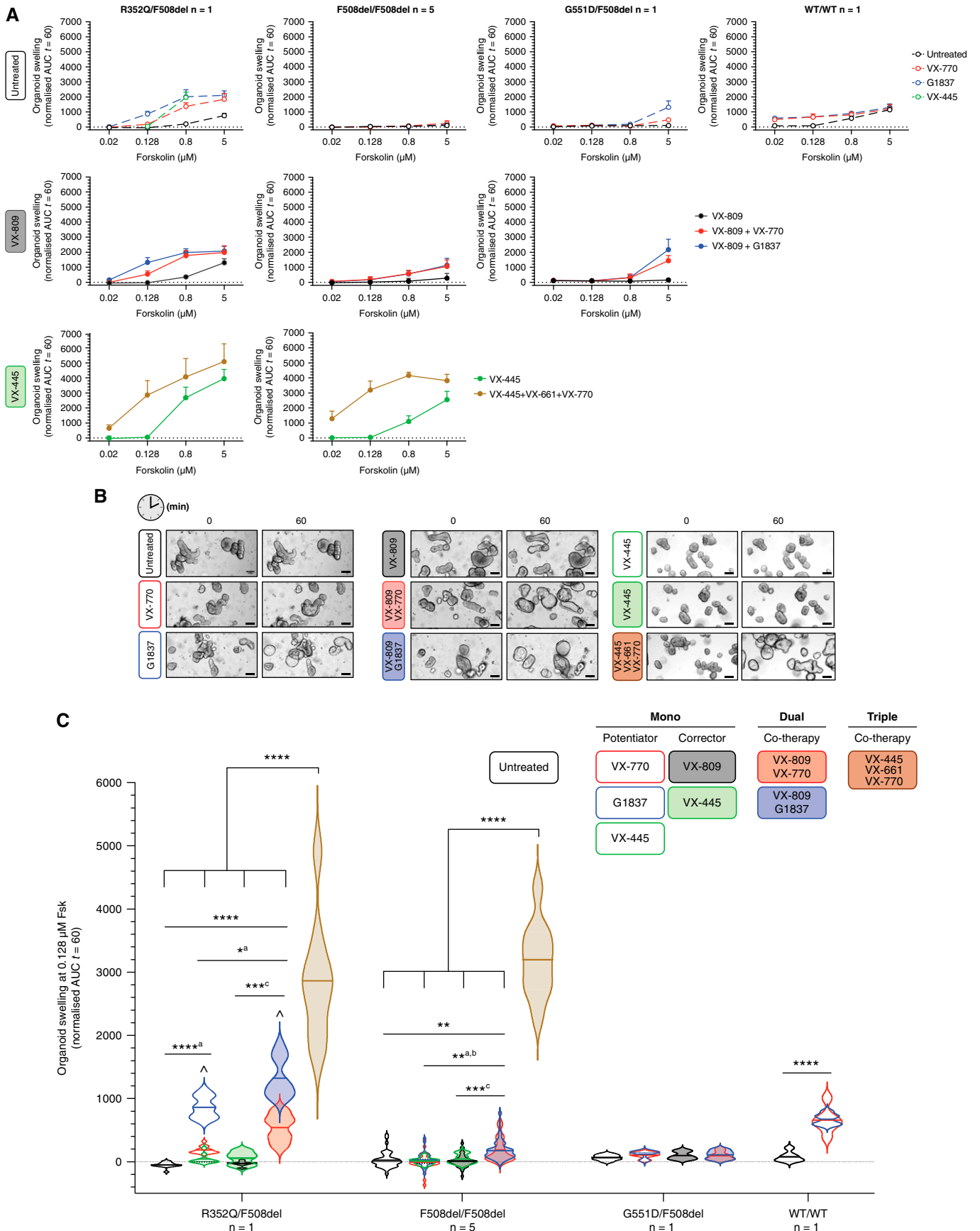


Figure 2. Functional response of R352Q-CFTR to CFTR modulators in intestinal organoids. Forskolin-induced swelling (FIS) assay in organoids (left to right) from one R352Q/F508del participant, five F508del/F508del participants, and one G551D/F508del participant with CF and one

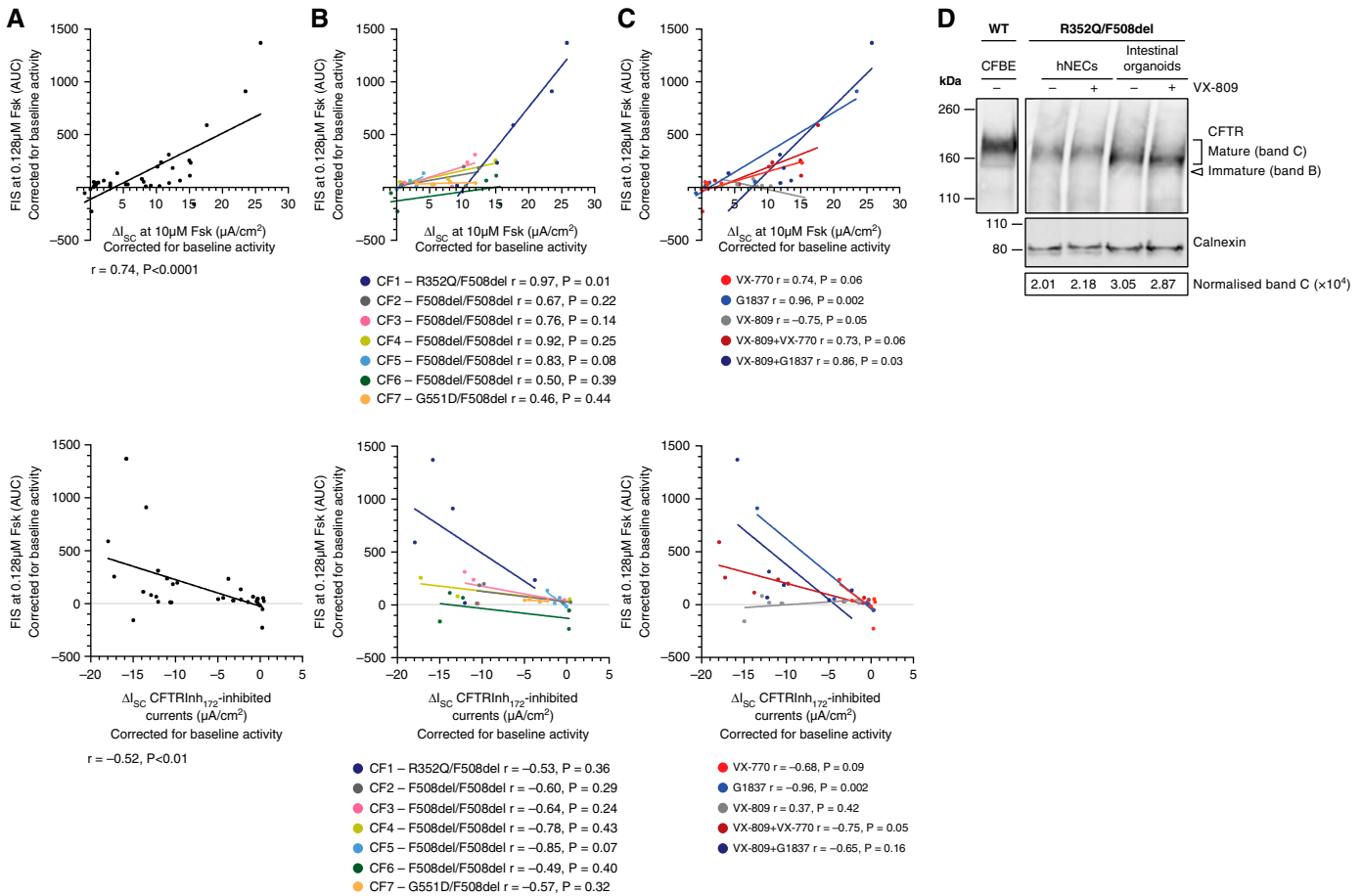


Figure 3. Correlation between individual *in vitro* treatment-modulated CFTR function in participant-matched differentiated hNECs and intestinal organoids. Modulator-enhanced CFTR response (top) and CFTRinh-172-inhibited response (bottom), corrected for the baseline CFTR activity, in hNECs (ΔI_{sc}) compared with organoids (FIS) from each participant shown (A) as a collective, (B) by participant, and (C) by modulator therapy. The lines through data points show simple linear regression analysis. Correlation (r) values were calculated using Pearson linear correlation. (D) Western blot in lysates from R352Q/F508del hNECs and intestinal organoids following 48-hour treatment with DMSO (vehicle) or VX-809. Cell lysates of WT-CFTR human CF bronchial epithelial (CFBE41o-) cell line were used as a control for CFTR bands B and C protein size. Densitometry was calculated by measuring the level of mature mutant CFTR (band C) normalized to the calnexin loading control. Band C represents the mature, complex-glycosylated CFTR. Band B represents the immature, core-glycosylated CFTR.

organoids expressed a higher abundance of mature CFTR protein relative to the hNECs (~1.5 times), consistent with known CFTR enrichment in the human gallbladder, intestine, and pancreas (28, 29).

Molecular Dynamics Simulations and Free Energy Calculations Reveal the Dysfunction of the R352Q Mutant

We next characterized the structural defect of R352Q-CFTR with molecular dynamics (MD) simulations, using an extended model

of the phosphorylated, ATP-bound human CFTR (30). In line with the previously proposed role for R352 in forming a salt bridge (31), it was observed that mutation of the positively charged arginine (R) to neutral glutamine (Q) disrupted the R352-D993 salt

Figure 2. (Continued). WT-CFTR control participant. Organoids were incubated overnight with 0.03% DMSO (vehicle) or 3 μM VX-809 or 3 μM VX-445 or 3 μM VX-445 + 18 μM VX-661. After 24 hours, a range of Fsk concentrations from 0.02 to 5 μM were acutely added, either alone or in combination with 3 μM VX-770 (red) or 3 μM G1837 (blue) or 3 μM VX-445 (green). (A) Values plotted are the mean ± SD of the area under the curve (AUC). (B) Representative brightfield images of R352Q/F508del organoids at baseline ($t = 0$) and after 1 hour of stimulation ($t = 60$) at 0.128 μM Fsk. Scale bars, 100 μm. (C) Violin plots of FIS response (AUC at 0.128 μM Fsk) of organoids from participants with CF and WT-CFTR control participants, expressed as the absolute AUC calculated from the time periods $t = 0$ (baseline) to $t = 60$. Data are represented as violin plots to show the distribution of data. n , number of participants. One-way ANOVA was used to determine statistically significant differences. * $P < 0.05$, ** $P < 0.01$, *** $P < 0.001$, and **** $P < 0.0001$. ^a P for G1837 only, ^b P for VX-770 only, ^c P for VX-809 only, and ^d P for G1837 versus VX-770 or VX-445. Where VX-770, G1837, and VX-445 (overlapping violin plots) achieved statistical significance, the least significant P value is shown.

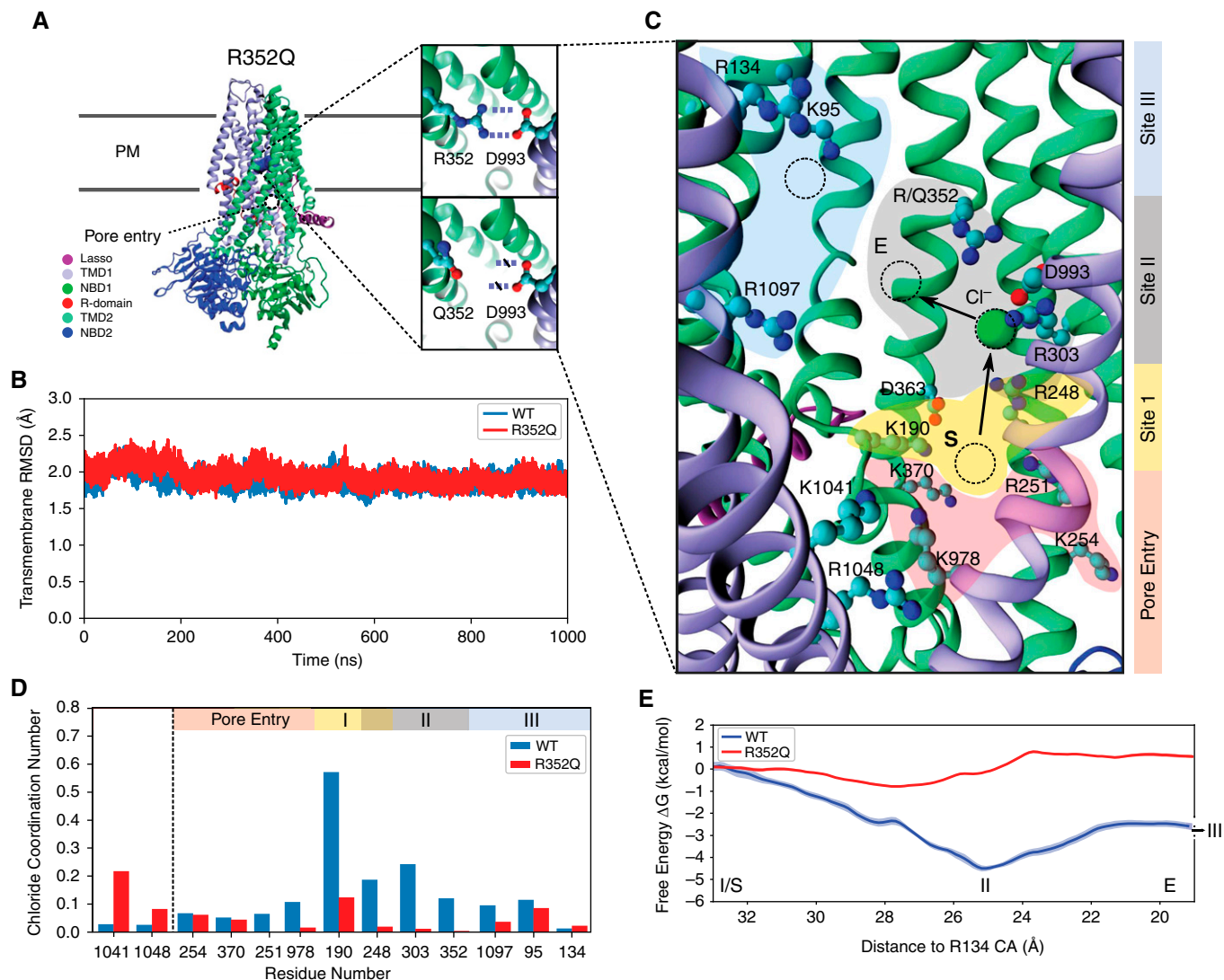


Figure 4. Simulations provide a mechanistic understanding of R352Q-CFTR dysfunction. (A) Atomistic structure of the CFTR channel pore based on cryo-EM (6MSM), with the configuration of the R352-D993 salt bridge and the disrupted R352Q highlighted in insets. Mutation of the charged R352 side chain (right top) to the neutral Q352 side chain (right bottom) disrupts the R352-D993 salt bridge present in WT-CFTR. (B) The root-mean-squared deviations (RMSDs) of the transmembrane domains of WT-CFTR (blue) and R352Q-CFTR (red) channel pore, computed using the 6MSM coordinates as reference. (C) A visualization of charged residues that line the CFTR channel pore. The path of chloride ion conduction from pore entry (pink) to site I (yellow), site II (gray), and site III (blue) is indicated. The computed free energy path in (E) is defined with reference to the chloride ion's distance to the α -carbon of R134 in site III, with the start and end points delineated by S and E, respectively. Charged residues lining the channel pore are shown as ball and sticks. An example chloride ion is represented with a green ball in site II. (D) The histogram shows the chloride ion occupancy in WT-CFTR (blue) and R352Q-CFTR (red). The number of chloride ions within 4 Å of the sidechain nitrogen atoms of the residue in each frame of the trajectory was counted and divided by the total number of frames. (E) Free energy profile of a chloride ion in the WT-CFTR (blue) and R352Q-CFTR (red) channel pore. The change in free energy relative to site I is plotted versus the chloride ions distance to the α -carbon of R134 (site III). NBD, nucleotide-binding domain; PM, plasma membrane; R-domain, regulatory domain; TMD, transmembrane domain.

bridge in the midsection of the CFTR channel pore (Figure 4A, Figure E4). This salt bridge is a key structural element in CFTR, and its disruption has been shown to impact conductance and gating (31). However, there was no discernible disruption to the R352Q-CFTR channel pore architecture, because the root mean squared

deviations of membrane-spanning helices of the R352Q-CFTR were as stable as the WT in microsecond-long MD simulations (Figure 4B). This suggests that the R352Q-CFTR open conformation can remain stable on the submicrosecond time scale necessary for chloride conduction (32). If gating was impacted by the R352Q mutation, longer

simulations might be able to decipher any disrupted pore architecture.

Because the R352 residue lines the CFTR channel pore, the R352Q mutation can be expected to affect the conduction of chloride ions (33). This was assessed by determining the path of chloride conduction through the channel and comparing the

occupancy of residues along the conduction pathway in WT-CFTR and R352Q-CFTR (Figures 4C and 4D, Video E2). In the WT system, a chloride ion spontaneously enters the pore intracellular gate (34) and diffuses toward K190 and K370 (site I) (Figure 4C). It remains in this site for ~ 10 nanoseconds and then spontaneously moves up to the vicinity of R352 and R303 (site II). R248, which is positioned between sites I and II, coordinates the chloride ion movement between these sites. The chloride ion then moves to the vicinity of R134 and K95 (site III), which coordinate chloride diffusion into the outermost section of CFTR. Chloride conduction through the CFTR channel pore does not follow a straight path from pore entry to site III but rather follows a longer, indirect route. This is in contrast to the straight path that ions follow through voltage-gated potassium and sodium channels, which have tight pores that run perpendicular to the membrane (35).

In R352Q-CFTR, chloride ions can enter the channel pore but not as readily as in the WT system. They also generally do not progress as far into the pore as for WT-CFTR. Although multiple chloride ions occupied the WT-CFTR channel pore concurrently, only one chloride ion at a time was observed in the R352Q-CFTR channel pore. The highest occupancy in R352Q-CFTR was found for K1041. The chloride ions that enter the WT-CFTR channel pore stayed mainly in sites I and II, with occupancies of these two sites drastically reduced in R352Q-CFTR compared with WT-CFTR. This reduction in occupancy observed in R352Q-CFTR is due to neutralization of the positively charged R352 side chain, which reduces the affinity of chloride ions to site II. Site III was inadequately sampled to draw conclusions (Figure 4D). Intriguingly, some chloride ions appeared to penetrate site III in both WT- and R352Q-CFTR, which could explain the mild conductance defect observed for R352Q. In addition, in simulations of WT-CFTR, it was observed that D993 alternated contact between R303 and R352 (Figures E4A and E4B). However, in R352Q-CFTR, D993 forms a more stable salt bridge with R303 (Figure E4C), which curtails its ability to coordinate a chloride ion.

The impact of the lower occupancy of sites I and II on chloride conductance was quantified further by comparing the respective free energy profiles obtained from umbrella sampling MD simulations

(Figure 4E). To generate the initial path for the umbrella sampling simulations, one chloride ion was constrained at site I and then steered via site II toward R134 in site III, using a moving restraint. The free energy profile calculations followed the protocol described in the SUPPLEMENTAL MATERIALS AND METHODS of the data supplement. In WT-CFTR, calculation of the free energy profile yielded an energy trough of -4 kcal/mol at site II relative to site I (Figure 4E). This indicates that chloride ions will be attracted to this site. In contrast, in R352Q-CFTR, the free energy profile exhibited an energy barrier of $+1$ kcal/mol at site II, which will likely hinder chloride conduction. Therefore, in WT-CFTR, a chloride ion in site I will tend to move to site II, whereas such a motion will be suppressed in R352Q-CFTR, resulting in reduced chloride conductance.

Discussion

This study adds to previously published findings by other CF laboratories by validating the reproducibility of cell models created from participants with CF for assessment of CFTR activity via *in vitro* CFTR functional assays (17, 21). To characterize the rare R352Q-CFTR mutation, we first created matched hNECs and intestinal organoids from participants with CFTR mutations that have known functional defects. These acted as references in the functional assays, and because these reference mutations are common to other published platforms (17, 21), this facilitated comparison of data from our functional platform. Our reference hNECs and organoids both showed similar patterns of response to modulators when compared with previous studies, although the magnitude of response is lower (17, 19, 21, 24). Variabilities in the magnitude of CFTR response in cell models created from different laboratories are evident (Figure E5). This could be attributed to several reasons. First, CFTR functional response to modulators in patient cell models was shown to be significantly modified by minor alterations to the culture media (36, 37). Patient-to-patient variability in CFTR response may also explain this observation (19, 38, 39), which could be further skewed if a relatively small number of participants are studied. The variabilities in data between laboratories highlight the necessity to create reference cell models at every test center for comparison and characterization of rare CFTR genotypes.

To date, R352Q-CFTR functional characterization has been performed only in heterologous expression Chinese hamster ovary, Fischer rat thyroid and CFBE41o– cells (25, 40, 41). These studies demonstrate varying levels of baseline activity ranging from 3% to 20% of WT-CFTR. However, *in vivo* CFTR function measured using nasal potential difference has shown that an individual with the R352Q/G1244E-CFTR genotype had CFTR activity just below that of WT individuals (19). The G1244E mutation is a CFTR gating mutation with severe defect (42), suggesting that R352Q confers high levels of CFTR activity. To better characterize the R352Q mutation, we assessed CFTR function in hNECs and organoids derived from a R352Q/F508del-CFTR participant. Of the 100 individuals bearing the R352Q mutation in the CFTR2 database, 99 are heterozygous with F508del or another CFTR mutation genotype (42). Therefore, our study participant is an appropriate representative of the R352Q-CFTR population.

The CFTR activity of a mutation is commonly expressed as a percentage of WT-CFTR activity to measure the severity of defect and responsiveness to modulator (19, 40). However, we noted limitation in its use because WT-CFTR activity is somewhat underestimated in hNECs, resulting in overestimation of mutant CFTR activity. Baseline CFTR activity in R352Q/F508del hNECs was 70% of WT-CFTR activity. This was potentiated to well above WT-CFTR activity by VX-770 and G1837. Underestimation of the WT-CFTR activity was also shown by Pranke and colleagues (19), who showed that VX-770-potentiated CFTR current for R352Q/G1244E hNECs was $\sim 160\%$ of the WT-CFTR activity (19). In our study, we found that the WT hNECs had significantly higher resting I_{sc} than the CF hNECs (WT, $27.5 \pm 1.5 \mu\text{A}/\text{cm}^2$ vs. CF, $1.1 \pm 0.7 \mu\text{A}/\text{cm}^2$; $P < 0.0001$; data not shown), suggesting that there was endogenous CFTR activity at resting state even without the presence of Fsk. This may have limited further chloride transport when the cells were stimulated with Fsk, underestimating the WT-CFTR activity. The presence of endogenous CFTR activity is also evident in WT intestinal organoids, which were reported to have preswollen morphology at resting state in the absence of Fsk (17). Notably, a recent study reported that patient-derived cell models are effective tools to identify modulator-responsive patients but may not

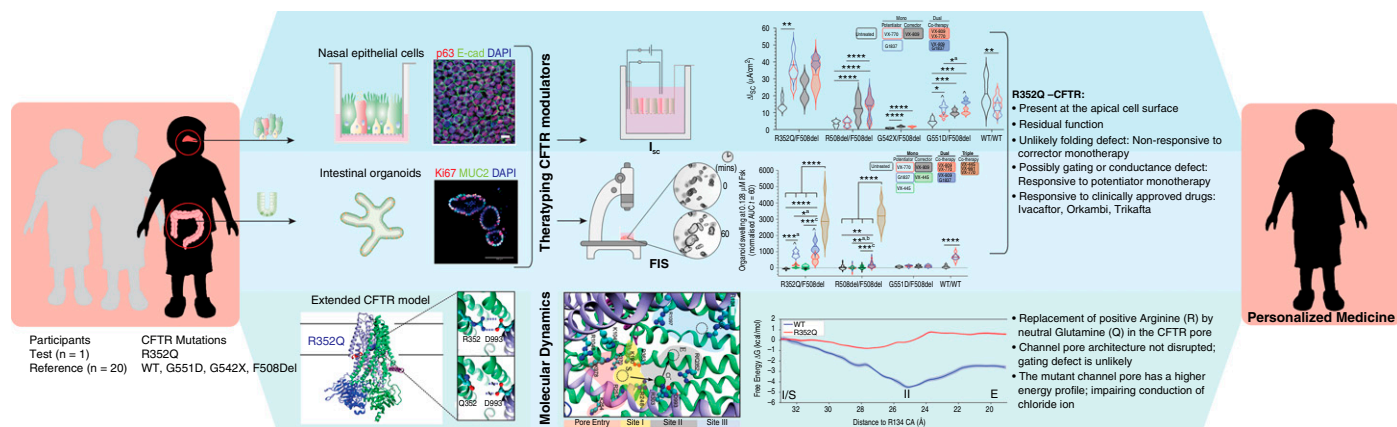


Figure 5. Flowchart demonstrating functional and *in silico* experiments for characterization of the R352Q-CFTR and summary of major findings.

accurately predict the magnitude of clinical benefit (43). It is likely that although the percentage of WT-CFTR activity is useful as a guide of reference for CFTR functional rescue, *in vitro* and *in vivo* CFTR function do not correlate in a linear fashion.

Nonetheless, the high baseline I_{sc} ($14.8 \mu\text{A}/\text{cm}^2$) and FIS (AUC, 196.3) of R352Q indicates a discernible amount of functional CFTR is present at the cell surface. In support of this, VX-809 monotherapy did not further improve CFTR activity in either R352Q/F508del hNECs or organoids. This is consistent with findings that VX-809 treatment did not further improve VX-770-potentiated CFTR activity in R352Q/G1244E hNECs (19). Western blot analysis in Fischer rat thyroid and CF bronchial epithelial cells showed that 80–98% of R352Q-CFTR is present as mature CFTR localized to the cell surface, with little evidence of a processing or turnover defect (40, 41). For this reason, because the mechanism of action of VX-809 is correction of a folding defect in CFTR that disrupts its trafficking to the cell surface, it is expected to have little, if any, restorative effect on R352Q-CFTR (44). Our functional data confirm previous reports that the R352Q mutation is unlikely to cause folding defects and suggests that patients with R352Q-CFTR are unlikely to benefit from corrector modulator monotherapy.

Single-channel and whole-cell patch-clamp studies have demonstrated that the positively charged arginine (R352) creates an electropositive potential that promotes anion movement through the channel pore (25). In addition, R352 forms a salt bridge with the negatively charged D993 residue (TM9), and this interaction is critical to keep the CFTR

channel pore in a stable open-pore state (45). Our MD simulations performed on the extended structure of human CFTR (Protein Data Bank accession no. 6MSM) also showed that R352Q disrupts the R352-D993 salt bridge in the channel pore; however, the gross architecture of the channel pore was unchanged. We showed that the R352 residue is not essential for chloride ion entry into the channel pore but is necessary to maintain chloride ion occupancy at a binding site within the channel pore conductance pathway (site II) for normal chloride ion conductivity. This is consistent with previous studies demonstrating that R352Q caused frequent transitioning of the channel pore to subconductance states (~40–70%) and occasional full conductance channel pore opening (31, 46), causing a mild conductance defect. In the same studies, no apparent reduction in channel pore open probability (P_o) was deduced or reported from the single-channel patch-clamp recordings, suggesting a gating defect was unlikely. This is consistent with our MD simulations that predicted the R352Q open conformer can remain stable during chloride ion conduction.

The exact mechanism of action of CFTR potentiators VX-770 and G1837 is not fully understood. There is evidence that VX-770 rescues gating defects by enhancing P_o and stabilizing the open-pore conformation (47). VX-770 was initially approved for CFTR gating defects (48). In some countries, approval has since been extended to conductance defects, based at least in part on *in vitro* functional assays (40, 49). In principle, potentiators can enhance CFTR activity by increasing the opening time of channels (P_o) and/or

increasing channel conductance. It is plausible that the significant responsiveness of R352Q/F508del to potentiators was due to an increase in channel pore opening time. This extra time compensates for the energy barrier created by the R352Q mutation, which hinders chloride ion conduction.

Because CF is a multiorgan disease (50), we questioned if the response to modulator therapy in both lung- and intestine-derived cell models from the same individual would be similar. Overall, our data indicated a positive correlation between CFTR functional response to modulators in matched hNECs and organoids across all CFTR mutations assayed. This is consistent with recent findings in several other rare CFTR mutations, such as G85E, P205S, and D614G (51). In our study, among all modulators, VX-809 monotherapy was the only therapy to result in a negative correlation in response between the two cell models in all participants. The hNECs of all participants were responsive to VX-809 monotherapy but not their intestinal organoids. We propose two mechanisms that could result in this discrepancy. First, the VX-809 incubation time of 24 hours in organoids is shorter than the 48 hours in hNECs. This could impact the number of F508del-CFTR that are successfully trafficked from the endoplasmic reticulum to the cell surface because this correction is a time-dependent process (52). In addition to having a trafficking and gating defect, F508del-CFTR is less stable at the cell surface (53). Therefore, the shorter VX-809 incubation period in organoids may negatively impact CFTR stabilization at the cell surface.

Another mechanism could be the different concentration of Fsk used between the two assays. Both the I_{sc} and FIS assays use Fsk to stimulate protein kinase A-dependent CFTR activation (54, 55). Protein kinase A increases channel P_o in a dose-dependent manner (56). FIS at 0.128 μ M Fsk correlates best with *in vivo* lung function (percent predicted FEV₁) and allows characterization of responses in organoids without reaching ceiling threshold (saturation) in high residual function *CFTR* mutations (17). In contrast, 10 μ M Fsk has been the default concentration for I_{sc} measurements since early reports of this technique (57, 58). However, it has recently been shown that 3 μ M Fsk is sufficient to saturate the CFTR response in hNECs (59). The high concentrations of Fsk in the I_{sc} assay are likely to function like a potentiator, extending CFTR channel opening time (56). This might explain the significant response to VX-809 monotherapy we observed in hNECs but not in matching organoids that were treated with a nearly 100-fold lower concentration of Fsk (0.128 μ M).

Strengths and Limitations

A strength of our study is the cross-validation of modulator response in matched hNECs and intestinal organoid cultures

derived from the same participants. This minimizes the possibility of cell culture-dependent bias. We could not correlate *in vitro* CFTR response to participant *in vivo* clinical response, because individuals under 12 years of age with an R352Q-*CFTR* mutation in Australia do not currently have access to CFTR modulator therapy.

MD simulation studies are emerging as a method to understand the molecular mechanism by which rare mutations cause the CFTR protein to malfunction (60). The combination approach of using *in vitro* experiments and MD simulations to characterize the R352Q-*CFTR* mutation paves a feasible and reliable pathway to personalized therapies for participants with rare *CFTR* mutations (Figure 5). In our simulations, we demonstrated that alterations to the free energy profile in the channel pore introduced as a result of the R352Q mutation negatively impacted movement of the chloride ions to move past the midpoint of the CFTR channel pore (site II), diminishing the channel's conductance. *In vitro* experiments complement these simulations by demonstrating that the unique defect introduced by a mutation can be rescued by CFTR modulators (61–63). In this study, we have demonstrated that the

R352Q-*CFTR* defect is rescued by potentiators. Functional characterization of CFTR in both lung and intestinal models may improve the specificity and sensitivity of predicting modulator test results and aid in translating patient-derived cell models to become a mainstream companion diagnostic test for people with CF. ■

Author disclosures are available with the text of this article at www.atsjournals.org.

Acknowledgment: The authors thank the study participants and their families for their contributions. The authors also thank Sydney Children's Hospitals Randwick respiratory department, especially Dr. Yvonne Belessis, Leanne Plush, Amanda Thompson, and Rhonda Bell, in the organization and collection of participant biospecimens. The authors thank Nihan Turgutoglu for culture and maintenance of primary cells. The authors thank Dr. Alexander Capraro for transferring manuscript figures to Adobe Illustrator. The authors acknowledge the Hubrecht Institute for the generous provision of the L-Wnt3A cell line. Computations were performed on the gadi HPC at the National Computational Infrastructure in Canberra and Artemis at the Sydney Informatics Hub in The University of Sydney. The authors thank Dr. John R. Riordan (University of North Carolina at Chapel Hill) and the Cystic Fibrosis Foundation for providing anti-CFTR antibody 596.

References

- Rusekkaite R, Ahern S, Ranger T, Dean J, Gardam M, Bell S, *et al.*; Australian Cystic Fibrosis Data Registry. The Australian Cystic Fibrosis Data Registry Annual Report 2017. Melbourne, Australia: Monash University, Department of Epidemiology and Preventive Medicine; March 2019. Report No. 20 [accessed 2021 Jun 30]. Available from: https://www.cysticfibrosis.org.au/getmedia/24e94d66-29fa-4e3f-8e65-21ee24ed2e5a/ACFDR-2017-Annual-Report_highres_singles.pdf.
- Saint-Criq V, Gray MA. Role of CFTR in epithelial physiology. *Cell Mol Life Sci* 2017;74:93–115.
- Marson FAL, Bertuzzo CS, Ribeiro JD. Classification of CFTR mutation classes. *Lancet Respir Med* 2016;4:e37–e38.
- Clancy JP, Cotton CU, Donaldson SH, Solomon GM, VanDevanter DR, Boyle MP, *et al.* CFTR modulator therotyping: current status, gaps and future directions. *J Cyst Fibros* 2019;18:22–34.
- Loo TW, Bartlett MC, Clarke DM. Corrector VX-809 stabilizes the first transmembrane domain of CFTR. *Biochem Pharmacol* 2013;86:612–619.
- Ren HY, Grove DE, De La Rosa O, Houck SA, Sopha P, Van Goor F, *et al.* VX-809 corrects folding defects in cystic fibrosis transmembrane conductance regulator protein through action on membrane-spanning domain 1. *Mol Biol Cell* 2013;24:3016–3024.
- Shaughnessy CA, Zeitlin PL, Bratcher PE. Elexacaftor is a CFTR potentiator and acts synergistically with ivacaftor during acute and chronic treatment. *Sci Rep* 2021;11:19810.
- Laselva O, Bartlett C, Gunawardena TNA, Ouyang H, Eckford PDW, Moraes TJ, *et al.* Rescue of multiple class II CFTR mutations by elexacaftor+tezacaftor+ivacaftor mediated in part by the dual activities of elexacaftor as both corrector and potentiator. *Eur Respir J* 2021;57:2002774.
- Veit G, Vaccarin C, Lukacs GL. Elexacaftor co-potentiates the activity of F508del and gating mutants of CFTR. *J Cyst Fibros* 2021;20:895–898.
- Okiyoneda T, Veit G, Dekkers JF, Bagdany M, Soya N, Xu H, *et al.* Mechanism-based corrector combination restores Δ F508-CFTR folding and function. *Nat Chem Biol* 2013;9:444–454.
- U.S. Food and Drug Administration (FDA). FDA approves new breakthrough therapy for cystic fibrosis [press release]. 2019 Oct 21 [accessed 2021 Jun 30]. Available from: <https://www.fda.gov/news-events/press-announcements/fda-approves-new-breakthrough-therapy-cystic-fibrosis>.
- U.S. Food and Drug Administration (FDA). FDA approves Symdeko (tezacaftor/ivacaftor and ivacaftor) to treat the underlying cause of cystic fibrosis in people ages 12 and older with certain mutations in the CFTR gene [press release]. 2018 Feb 12 [accessed 2021 Jun 30]. Available from: <https://investors.vrtx.com/news-releases/news-release-details/fda-approves-symdeko-tm-tezacaftorivacaftor-and-ivacaftor-treat>.
- U.S. Food and Drug Administration (FDA). FDA approves Orkambi (lumacaftor/ivacaftor) - the first medicine to treat the underlying cause of cystic fibrosis for people ages 12 and older with two copies of the F508del mutation [press release]. 2015 Jul 2 [accessed 2021 Jun 30]. Available from: <https://investors.vrtx.com/news-releases/news-release-details/fda-approves-orkambitm-lumacaftorivacaftor-first-medicine-treat>.
- Cystic Fibrosis Foundation. FDA approves expansion of modulators for people with certain rare mutations. 2020 Dec 21 [accessed 2021 Jun 30]. Available from: <https://www.cff.org/news/2020-12/fda-approves-expansion-modulators-people-certain-rare-mutations>.
- Bell SC, Mall MA, Gutierrez H, Macek M, Madge S, Davies JC, *et al.* The future of cystic fibrosis care: a global perspective. *Lancet Respir Med* 2020;8:65–124.

16. Clarke LA, Sousa L, Barreto C, Amaral MD. Changes in transcriptome of native nasal epithelium expressing F508del-CFTR and intersecting data from comparable studies. *Respir Res* 2013;14:38.
17. Dekkers JF, Berkers G, Kruisselbrink E, Vonk A, de Jonge HR, Janssens HM, et al. Characterizing responses to CFTR-modulating drugs using rectal organoids derived from subjects with cystic fibrosis. *Sci Transl Med* 2016;8:344ra84.
18. Martinovich KM, Iosifidis T, Buckley AG, Looi K, Ling KM, Sutanto EN, et al. Conditionally reprogrammed primary airway epithelial cells maintain morphology, lineage and disease specific functional characteristics. *Sci Rep* 2017;7:17971.
19. Pranke IM, Hatton A, Simonin J, Jais JP, Le Pimpec-Barthes F, Carsin A, et al. Correction of CFTR function in nasal epithelial cells from cystic fibrosis patients predicts improvement of respiratory function by CFTR modulators. *Sci Rep* 2017;7:7375.
20. Dekkers JF, van der Ent CK, Beekman JM. Novel opportunities for CFTR-targeting drug development using organoids. *Rare Dis* 2013;1:e27112.
21. Ramalho AS, Fürstová E, Vonk AM, Ferrante M, Verfaillie C, Dupont L, et al.; Belgian Organoid Project. Correction of CFTR function in intestinal organoids to guide treatment of cystic fibrosis. *Eur Respir J* 2021;57:1902426.
22. McCarthy C, Brewington JJ, Harkness B, Clancy JP, Trapnell BC. Personalised CFTR pharmacotherapeutic response testing and therapy of cystic fibrosis. *Eur Respir J* 2018;51:1702457.
23. Berkers G, van Mourik P, Vonk AM, Kruisselbrink E, Dekkers JF, de Winter-de Groot KM, et al. Rectal organoids enable personalized treatment of cystic fibrosis. *Cell Rep* 2019;26:1701–1708.e3.
24. Pranke I, Hatton A, Masson A, Flament T, Le Bourgeois M, Chedeveigne F, et al. Might brushed nasal cells be a surrogate for CFTR modulator clinical response? *Am J Respir Crit Care Med* 2019;199:123–126.
25. Guinamard R, Akabas MH. Arg352 is a major determinant of charge selectivity in the cystic fibrosis transmembrane conductance regulator chloride channel. *Biochemistry* 1999;38:5528–5537.
26. Han ST, Rab A, Pellicore MJ, Davis EF, McCague AF, Evans TA, et al. Residual function of cystic fibrosis mutants predicts response to small molecule CFTR modulators. *JCI Insight* 2018;3:e121159.
27. van Barneveld A, Stanke F, Tamm S, Siebert B, Brandes G, Derichs N, et al. Functional analysis of F508del CFTR in native human colon. *Biochim Biophys Acta* 2010;1802:1062–1069.
28. Uhlén M, Fagerberg L, Hallström BM, Lindskog C, Oksvold P, Mardinoglu A, et al. Tissue-based map of the human proteome. *Science* 2015;347:1260419.
29. Human Protein Atlas. 2021 [accessed 2021 Jun 30]. Available from: <http://www.proteinatlas.org>.
30. Wong SL, Awatade NT, Astore MA, Allan KM, Camell MJ, Slapetova I, et al. Molecular dynamics and functional characterization of I37R-CFTR lasso mutation provide insights into channel gating activity. *iScience* 2021;25:103710.
31. Cui G, Zhang ZR, O'Brien AR, Song B, McCarty NA. Mutations at arginine 352 alter the pore architecture of CFTR. *J Membr Biol* 2008;222:91–106.
32. Sorum B, Czégé D, Csanády L. Timing of CFTR pore opening and structure of its transition state. *Cell* 2015;163:724–733.
33. Zhang Z, Liu F, Chen J. Molecular structure of the ATP-bound, phosphorylated human CFTR. *Proc Natl Acad Sci USA* 2018;115:12757–12762.
34. Linsdell P. Cystic fibrosis transmembrane conductance regulator (CFTR): making an ion channel out of an active transporter structure. *Channels (Austin)* 2018;12:284–290.
35. Flood E, Boiteux C, Lev B, Vorobyov I, Allen TW. Atomistic simulations of membrane ion channel conduction, gating, and modulation. *Chem Rev* 2019;119:7737–7832.
36. Awatade NT, Wong SL, Capraro A, Pandzic E, Slapetova I, Zhong L, et al. Significant functional differences in differentiated conditionally reprogrammed (CRC)- and feeder-free dual SMAD inhibited-expanded human nasal epithelial cells. *J Cyst Fibros* 2021;20:364–371.
37. Saint-Criq V, Delpiano L, Casement J, Onuora JC, Lin J, Gray MA. Choice of differentiation media significantly impacts cell lineage and response to CFTR modulators in fully differentiated primary cultures of cystic fibrosis human airway epithelial cells. *Cells* 2020;9:2137.
38. Matthes E, Goepp J, Martini C, Shan J, Liao J, Thomas DY, et al. Variable responses to CFTR correctors *in vitro*: Estimating the design effect in precision medicine. *Front Pharmacol* 2018;9:1490.
39. Brewington JJ, Filbrandt ET, LaRosa FJ III, Moncivaiz JD, Ostmann AJ, Strecker LM, et al. Brushed nasal epithelial cells are a surrogate for bronchial epithelial CFTR studies. *JCI Insight* 2018;3:e99385.
40. Van Goor F, Yu H, Burton B, Hoffman BJ. Effect of ivacaftor on CFTR forms with missense mutations associated with defects in protein processing or function. *J Cyst Fibros* 2014;13:29–36.
41. Veit G, Da Fonte DF, Avramescu RG, Premchandara A, Bagdany M, Xu H, et al. Mutation-specific dual potentiators maximize rescue of CFTR gating mutants. *J Cyst Fibros* 2020;19:236–244.
42. Clinical and Functional Translation of CFTR. CFTR2 database [accessed 2021 Jun 30]. Available from: <https://cftr2.org/>.
43. Kerem E, Cohen-Cymberek M, Tsabari R, Wilschanski M, Reiter J, Shoseyov D, et al. Ivacaftor in people with cystic fibrosis and a 3849 + 10kb C→T or D1152H residual function mutation. *Ann Am Thorac Soc* 2021;18:433–441.
44. Van Goor F, Hadida S, Grootenhuys PD, Burton B, Stack JH, Straley KS, et al. Correction of the F508del-CFTR protein processing defect *in vitro* by the investigational drug VX-809. *Proc Natl Acad Sci USA* 2011;108:18843–18848.
45. Cui G, Freeman CS, Knotts T, Prince CZ, Kuang C, McCarty NA. Two salt bridges differentially contribute to the maintenance of cystic fibrosis transmembrane conductance regulator (CFTR) channel function. *J Biol Chem* 2013;288:20758–20767.
46. Zhang J, Hwang TC. Electrostatic tuning of the pre- and post-hydrolytic open states in CFTR. *J Gen Physiol* 2017;149:355–372.
47. Jih KY, Lin WY, Sohma Y, Hwang TC. CFTR potentiators: from bench to bedside. *Curr Opin Pharmacol* 2017;34:98–104.
48. Vertex. FDA approves Kalydeco (ivacaftor), the first medicine to treat the underlying cause of cystic fibrosis [press release]. 2012 Jan 31 [accessed 2021 Jun 30]. Available from: <https://investors.vrtx.com/news-releases/news-release-details/fda-approves-kalydecom-ivacaftor-first-medicine-treat>.
49. Vertex. FDA approves Kalydeco (ivacaftor) for more than 900 people ages 2 and older with cystic fibrosis who have certain residual function mutations [press release]. 2017 May 17 [accessed 2021 Jun 30]. Available from: <https://investors.vrtx.com/news-releases/news-release-details/fda-approves-kalydeco-ivacaftor-more-900-people-ages-2-and?ReleaseID=1026864>.
50. Ratjen F, Bell SC, Rowe SM, Goss CH, Quittner AL, Bush A. Cystic fibrosis. *Nat Rev Dis Primers* 2015;1:15010.
51. Silva IAL, Railean V, Duarte A, Amaral MD. Personalized medicine based on nasal epithelial cells: comparative studies with rectal biopsies and intestinal organoids. *J Pers Med* 2021;11:421.
52. Jurkuvenaite A, Chen L, Bartoszewski R, Goldstein R, Bebek Z, Matalon S, et al. Functional stability of rescued delta F508 cystic fibrosis transmembrane conductance regulator in airway epithelial cells. *Am J Respir Cell Mol Biol* 2010;42:363–372.
53. Gentsch M, Chang X-B, Cui L, Wu Y, Ozols VV, Choudhury A, et al. Endocytic trafficking routes of wild type and DeltaF508 cystic fibrosis transmembrane conductance regulator. *Mol Biol Cell* 2004;15:2684–2696.
54. Dekkers JF, Wiegerinck CL, de Jonge HR, Bronsveld I, Janssens HM, de Winter-de Groot KM, et al. A functional CFTR assay using primary cystic fibrosis intestinal organoids. *Nat Med* 2013;19:939–945.
55. Gentsch M, Boyles SE, Cheluvharaju C, Chaudhry IG, Quinney NL, Cho C, et al. Pharmacological rescue of conditionally reprogrammed cystic fibrosis bronchial epithelial cells. *Am J Respir Cell Mol Biol* 2017;56:568–574.
56. Cui G, Stauffer BB, Imhoff BR, Rab A, Hong JS, Sorscher EJ, et al. VX-770-mediated potentiation of numerous human CFTR disease mutants is influenced by phosphorylation level. *Sci Rep* 2019;9:13460.
57. Blouquit S, Morel H, Hinrasky J, Naline E, Puchelle E, Chinet T. Characterization of ion and fluid transport in human bronchioles. *Am J Respir Cell Mol Biol* 2002;27:503–510.
58. Smith JJ, Welsh MJ. Fluid and electrolyte transport by cultured human airway epithelia. *J Clin Invest* 1993;91:1590–1597.

59. Avramescu RG, Kai Y, Xu H, Bidaud-Meynard A, Schnúr A, Frenkiel S, *et al.* Mutation-specific downregulation of CFTR2 variants by gating potentiators. *Hum Mol Genet* 2017;26:4873–4885.
60. Callebaut I, Hoffmann B, Lehn P, Mornon JP. Molecular modelling and molecular dynamics of CFTR. *Cell Mol Life Sci* 2017;74:3–22.
61. Sabusap CM, Joshi D, Simhaev L, Oliver KE, Senderowitz H, van Willigen M, *et al.* The CFTR P67L variant reveals a key role for N-terminal lasso helices in channel folding, maturation, and pharmacologic rescue. *J Biol Chem* 2021; 296:100598.
62. Billet A, Elbahnsi A, Jollivet-Souchet M, Hoffmann B, Mornon J-P, Callebaut I, *et al.* Functional and pharmacological characterization of the rare CFTR mutation W361R. *Front Pharmacol* 2020;11:295.
63. Molinski SV, Ahmadi S, Ip W, Ouyang H, Villella A, Miller JP, *et al.* Orkambi and amplifier co-therapy improves function from a rare CFTR mutation in gene-edited cells and patient tissue. *EMBO Mol Med* 2017; 9:1224–1243.